Acta Crystallographica Section D
Biological Crystallography
ISSN 0907-4449

S-SAD, Se-SAD and S/Se-SIRAS using Cu *Kα* radiation: why wait for synchrotron time?

Christopher T. Lemke,[a,b] G. David Smith[a,c] and P. Lynne Howell[a,b]*

[a]Structural Biology and Biochemistry, Research Institute, Hospital for Sick Children, 555 University Avenue, Toronto, Ontario, M5G 1X8, Canada, [b]Department of Biochemistry, Faculty of Medicine, University of Toronto, Medical Sciences Building, Toronto, Ontario, M5S 1A8, Canada, and [c]Hauptman–Woodward Medical Research Institute Inc., 73 High Street, Buffalo, New York 14203, USA

Correspondence e-mail: howell@sickkids.ca

Received 3 July 2002
Accepted 20 September 2002

The structure of *Escherichia coli* argininosuccinate synthetase (EAS) has been determined using S-SAD, Se-SAD and S/Se-SIRAS data measured with Cu *Kα* radiation. EAS contains 16 methionines and three cysteines in 455 amino acids. At a wavelength of 1.54 Å (Cu *Kα*), the native (S-Met) and derivative (Se-Met) proteins yield anomalous signals of approximately 0.86 and 1.6%, respectively. Highly redundant data were measured to 2.0 Å from native and derivative EAS crystals. All three structure determinations were carried out in a highly automated manner using *SnB* and *SOLVE*/*RESOLVE*. Despite the minute Bijvoet differences at 1.54 Å, the signal was sufficient to determine the heavy-atom substructure and produce high-quality electron-density maps in all three cases. These maps were readily interpretable by the *RESOLVE* automated building algorithm, which modeled greater than 75% of all three structures. The success of these methods has profound implications for crystallographers experiencing difficulty with heavy-atom incorporation or with limited access to a synchrotron source.

1. Introduction

Over the past decade, there has been a remarkable increase in the number of protein structures that have been solved using multiple anomalous diffraction (MAD) data in conjunction with selenomethionine-derivatized proteins (Deacon & Ealick, 1999). This technique eliminates many of the problems associated with multiple isomorphous replacement (MIR), such as heavy-metal screening and the lack of isomorphism, and the crystal and data quality of the heavy-atom derivatives. Given a crystal of a protein in which methionine has been replaced by selenomethionine, MAD data from one cryo-frozen crystal is typically measured at a synchrotron at the selenium edge (maximum f') and peak (maximum f'') wavelengths, as well as at a remote wavelength. The Se-atom substructure can be determined through the use of direct-methods programs such as *SnB* (Weeks & Miller, 1999) in conjunction with difference anomalous E values (Blessing & Smith, 1999), by *SHELXL*97 (Sheldrick & Schneider, 1997) or through the use of Patterson techniques as implemented in *CNS_SOLVE* (Brünger *et al.*, 1998) or *SOLVE* (Terwilliger & Berendzen, 1999). From the known phases of the substructure, treatment of the data as a special case of MIR (Ramakrishnan & Biou, 1997) usually results in an interpretable map.

In order to obtain the specific wavelengths required by the MAD experiment, radiation from a synchrotron must be used. An additional advantage of synchrotron radiation is the generation of higher resolution data owing to the increased X-ray flux. However, the disadvantages of using synchrotron radiation are the required travel, rushed experiments and

limited available time. A far better situation would be the ability to measure data at a home source with Cu $K\alpha$ radiation.

The first protein whose structure was solved using only the anomalous signal from sulfur at the Cu $K\alpha$ wavelength was that of crambin (Hendrickson & Teeter, 1981). In spite of this significant accomplishment, the use of the sulfur anomalous signal to obtain protein phases has only been revisited in the past few years. The majority of structures that have been determined using the sulfur anomalous signal have been solved at a wavelength of 1.77 Å (Gordon *et al.*, 2001; Liu *et al.*, 2000; Micossi *et al.*, 2002). Not only does this still require the use of a synchrotron, but an additional set of data must be measured at a shorter wavelength (*e.g.* 0.9 Å) in order to obtain data to the diffraction limit of the crystal. While the anomalous signal from sulfur from data measured at the Cu $K\alpha$ wavelength has been used to improve phases that were obtained from other atoms (Yang & Pflugrath, 2001), at present the only example of a structure solved at a wavelength of 1.54 Å (other than crambin) is that of lysozyme (Dauter *et al.*, 1999). In this case, the data were measured at a synchrotron, which improves the signal-to-noise ratio, and the anomalous signal from the ten S atoms in the protein was augmented by seven chloride ions in the ordered solvent shell around the protein.

While there are many positive aspects to the use of synchrotron radiation, the ability to use the anomalous signal from either a native sulfur-containing ($f'' = 0.557$ electrons) or a seleno-derivatized ($f'' = 1.137$ electrons) protein measured at home with Cu $K\alpha$ radiation either alone (Se-SAD, S-SAD) or in combination (Se/S-SIRAS) to determine protein phases could be a major benefit to many crystallographers. Although such experiments would require more time owing to the reduced X-ray flux compared with a synchrotron, data can be measured with minimal time restrictions and a high degree of redundancy.

C-terminally histidine-tagged *E. coli* argininosuccinate synthetase (EAS), the protein used in this work, is a homotetramer of ∼51 kDa subunits, each of which contains 16 methionine residues and three cysteine residues in a 455-amino-acid polypeptide. The protein crystallizes with approximately 55% solvent content in space group *I*222 and contains a single EAS monomer in the asymmetric unit. Reported below are results showing that Cu $K\alpha$ data obtained from crystals of EAS and/or its selenomethioninyl derivative are capable of producing interpretable electron-density maps *via* S-SAD, Se-SAD or S/Se-SIRAS.

2. Methods and results

2.1. Expression, purification and crystallization of native and derivative EAS

Native and derivative EAS proteins were expressed, purified and crystallized in a manner similar to that reported previously (Lemke *et al.*, 1999; Lemke & Howell, 2001, 2002). Briefly, native and selenomethioninyl EAS were recombinantly expressed in *E. coli*, purified by Ni^{2+}-affinity chromatography and crystallized using the hanging-drop vapor-diffusion technique. Native EAS was crystallized in a drop consisting of 50%(*v*/*v*) protein solution (10 mg ml^{-1} EAS, 25 m*M* MES pH 6.5, 150 m*M* guanidine hydrochloride, 2.5 m*M* ATP and 7.5 m*M* $MgCl_2$) and 50%(*v*/*v*) seed solution (1.8 *M* sodium/potassium phosphate, 100 m*M* MES pH 6.5 and 10^{-6} diluted microseed crystals), which was suspended over a 650 µl reservoir of precipitating solution (1.6 *M* sodium/potassium phosphate and 100 m*M* MES pH 6.5). Selenomethioninyl EAS was crystallized under similar conditions, with the addition of 1 m*M* DTT to the protein solution. In both cases, diffraction-quality crystals grew within one week.

Table 1
Data-collection statistics.

Values in parentheses refer to reflections in the outer resolution shell, 2.00–2.07 Å.

	S-Met EAS		Se-Met EAS	
Wavelength (Å)	1.54		1.54	
Resolution range (Å)	37.4–2.0		35.6–2.0	
Space group	*I*222		*I*222	
Unit-cell parameters				
a (Å)	79.90		79.22	
b (Å)	105.23		105.06	
c (Å)	126.87		127.23	
Completeness (%)	100		100	
Total data	1057927		1028992	
Bijvoets	Unmerged	Merged	Unmerged	Merged
Unique data	72902	36467	72478	36245
Redundancy	14.5	29.0	14.2	28.4
$\langle I/\sigma(I)\rangle$†	85.6 (26.34)	101.0 (35.1)	42.5 (9.9)	51.0 (12.6)
$I > 3\sigma(I)$ (%)	97.2 (94.2)	99.0 (98.1)	91.9 (77.7)	96.15 (88.5)
$R_{\rm merge}$‡ (%)	3.4 (10.2)	3.5 (10.5)	5.0 (19.8)	5.2 (20.2)

† $\langle I/\sigma(I)\rangle = \{\sum_i [I_i/\sigma(I_i)]\}/n$, where n is the total number of reflections. ‡ $R_{\rm merge} = \sum\sum_i |I_i - \langle I\rangle| / \sum I_i$, where $\langle I\rangle$ is the average intensity of equivalent reflections and the sum is extended over all measured observations for all unique reflections.

2.2. Collection of 2.0 Å native and derivative EAS Cu $K\alpha$ data

A native EAS crystal (0.4 × 0.3 × 0.2 mm) and a selenomethioninyl EAS crystal (0.3 × 0.3 × 0.2 mm) were soaked for approximately 10 min in cryoprotectant solution (350 mg ml^{-1} trehalose, 1.3 *M* sodium/potassium phosphate, 75 m*M* MES pH 6.5, 150 m*M* guanidine hydrochloride, 2.5 m*M* ATP and 7.5 m*M* $MgCl_2$) and then transferred on a rayon CryoLoop (Hampton Research) to a continuous cold stream at 100 K and irradiated with Cu $K\alpha$ X-rays from an RU-H3R generator. For each crystal, 1440 0.5° φ-scanning images were collected in a single pass using an R-AXIS IV^{++} image-plate detector. No attempt was made to align the crystals for simultaneous measurement of Bijvoet-related reflections. The data were processed using the *d*TREK* program package (Pflugrath, 1999), with the reflections of a Bijvoet pair treated either as separate or as identical reflections during scaling and merging. Owing to a detector malfunction, a 15° wedge of Se-Met data was omitted, resulting in marginally less derivative data than native data. The data-collection and reduction statistics of both data sets are summarized in Table 1. Bayesian statistical expectation values were applied to both data sets using the

program *BAYES* (Blessing, 1989) prior to their use in *SOLVE* and structure refinement (§2.4 and §2.5, respectively).

2.3. Substructure determination using *SnB*

2.3.1. Sulfur SAD. The native data (Blessing, 1989) were processed using the *DREAR* program package. *DIFFE*, the final program of the suite, was used to calculate the anomalous difference *E* magnitudes of all reflections (Blessing & Smith, 1999). The 760 largest difference *E* magnitudes were used by *SnB* to generate a total of 7600 triple invariants. Each of 10 000 trials contained 19 random starting-atom positions (16 S atoms from methionine and three from cysteine) and each trial structure was subjected to 38 cycles of phase refinement using the parameter-shift method (90° phase shift, two shifts, three passes). For all other parameters, the defaults were taken as recommended in Howell *et al.* (2000). The resulting distribution of the minimal function, $R_{\rm min}$, was bimodal and identified 17 potential solutions (Fig. 1). The solutions were analyzed using the program *NANTMRF* (Smith, 2002), which compared the atomic positions among the solutions, allowing for all possible combinations of enantiomorph, symmetry and origin of the space group. Each of the 17 potential solutions contained 15 absolutely conserved peak positions. The average position of each of the 15 sites was calculated and used in subsequent protein phase calculations (§2.4.2). Although the average site positions were used in this paper, the variation in site positions among the solutions was extremely low (mean displacement = 0.11 Å), suggesting that positions taken from any one of the 17 solutions would have been equally successful in phasing. When subsequently compared with the refined structures of EAS (§2.5), all 15 sites were determined to be correct sulfur positions.

2.3.2. Selenium SAD. The Se-Met data (unmerged Bijvoets) were used to determine the anomalously scattering substructure in a manner analogous to that described above (§2.3.1). The resulting distribution of $R_{\rm min}$ was bimodal with 248 potential solutions.

2.3.3. Sulfur/selenium SIR. The native and derivative data with merged Bijvoets were processed by *DREAR* to calculate

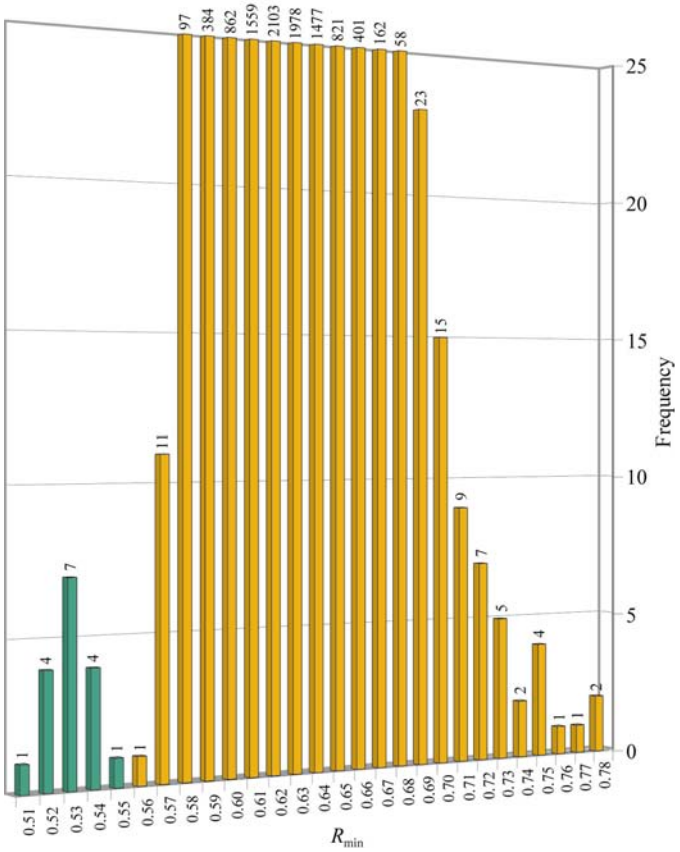

Figure 1
Histogram of $R_{\rm min}$ *versus* frequency for the sulfur *SnB* substructure determination. Solutions are colored green, while non-solutions are colored orange. For display purposes, the frequency axis has been truncated at 25. The number above each column indicates the total number of trials for that bin.

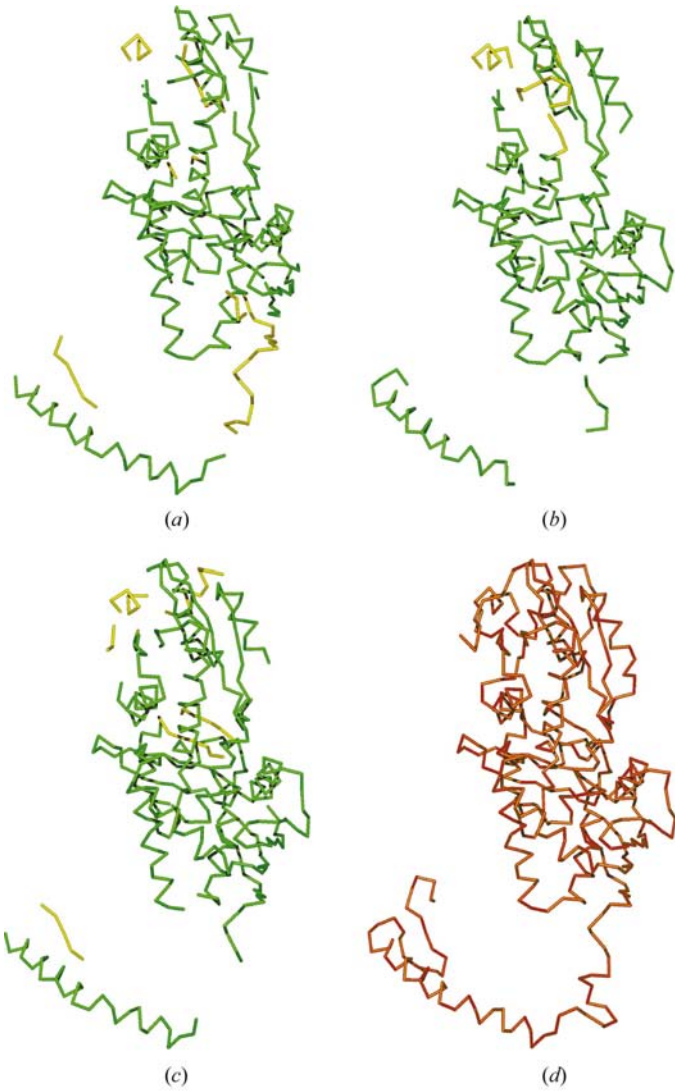

Figure 2
C^{α} traces of the *RESOLVE* models and known EAS structure. (*a*), (*b*) and (*c*) the *RESOLVE* S-SAD, Se-SAD and S/Se-SIRAS models, respectively. Residues modeled in full are colored green, while residues truncated to glycine or alanine are coloured yellow. (*d*) The native EAS structure (PDB ID 1k92).

isomorphous difference E magnitudes and used to determine the Se-atom substructure. The *SnB* procedure was identical to that used for the determination of the anomalous scattering substructure (§§2.3.1, 2.3.2), except that 800 difference E magnitudes were used to generate 7800 triple invariants and 16 random starting-atom positions were subjected to 32 cycles of phase refinement. The resulting distribution of $R_{\rm min}$ was again bimodal, identifying 44 potential solutions. Although the Se-atom positions identified by *SnB* Se-SAD and S/Se-SIR could have been used for subsequent protein phasing, *SOLVE* was equally capable of identifying the substructure (§§2.4.2, 2.4.3). Therefore, the Se-atom positions found by *SnB* Se-SAD and S/Se-SIR were not used in subsequent protein phase calculations.

2.4. Phase determination and automated model building using *SOLVE*/*RESOLVE*

2.4.1. *SOLVE*/*RESOLVE* strategy. *SOLVE* and *RESOLVE* were used to calculate protein phases and build initial models *via* S-SAD, Se-SAD and S/Se-SIRAS (§§2.4.2–2.4.4). For the structure determinations presented in this work, very basic *SOLVE* and *RESOLVE* input files were used; default parameters were taken where possible and no special cutoffs were applied to the data. Although a resolution cutoff was imposed by *SOLVE* for the calculation of initial phases in the S-SAD and Se-SAD cases, the phases were subsequently extended to 2.0 Å during the *RESOLVE* solvent-flattening and density-modification algorithms.

2.4.2. Sulfur SAD. The 15 S-atom positions determined by *SnB* S-SAD (§2.3.1) were used in conjunction with the SAD algorithm of *SOLVE* to calculate phase-probability distributions by exploiting the anomalous differences in the Cu $K\alpha$ S-Met EAS data. Although there are 19 S atoms in the protein, no additional S-atom positions were sought. The electron-density map obtained using the basic *SOLVE*/*RESOLVE* strategy described above was of sufficient quality for the automated model-building algorithm to correctly build 305 residues of the 446 residue protein (Table 2; Fig. 2).

2.4.3. Selenium SAD. The SAD algorithm of *SOLVE* was used to search for anomalous scattering atoms and calculate

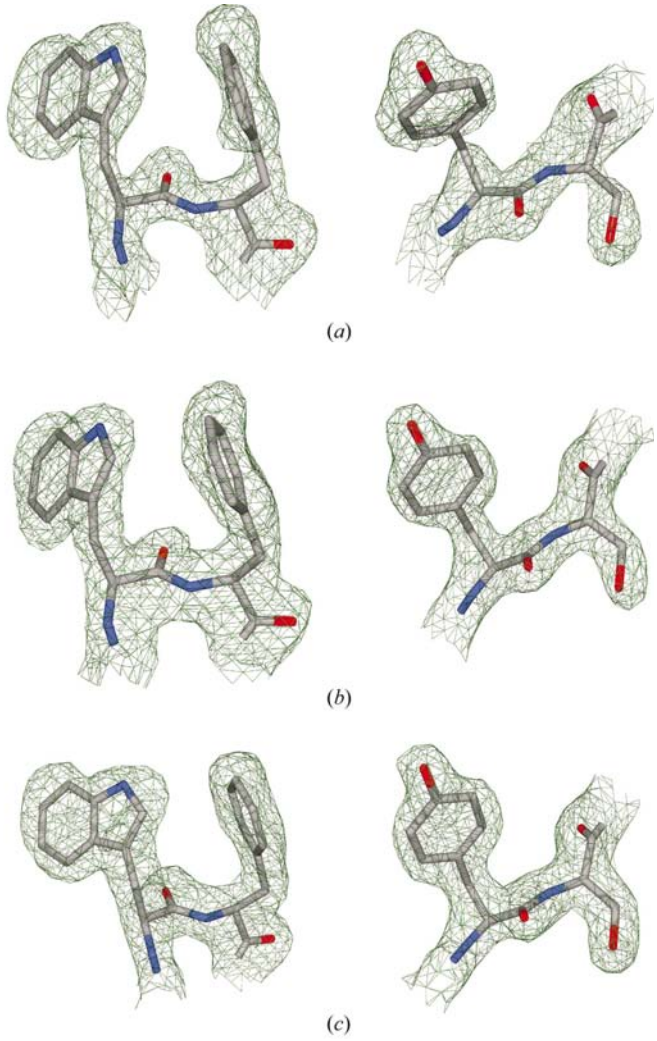

Figure 3
(*a*), (*b*) and (*c*) Sample solvent-flattened F_o electron density (contoured at 1.5σ) for the S-SAD, Se-SAD and S/Se-SIRAS structure determinations, respectively.

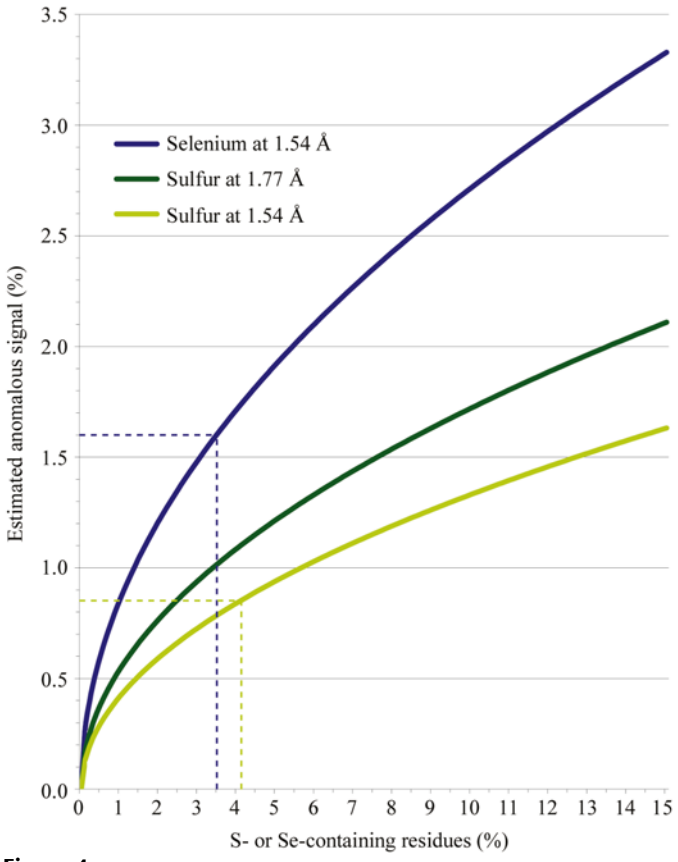

Figure 4
Plot of estimated anomalous signal *versus* protein sulfur/selenium content. The green and blue dotted lines indicate the sulfur and selenium anomalous scattering signals of S-Met and Se-Met EAS, respectively. The anomalous signal was calculated by $\langle \Delta F^{\pm} / F_T \rangle = (N_A/2N_T) - (2f''/Z_{\rm eff})$, where N_A and N_T are the number of anomalous scatters and the number of non-H atoms, respectively, f'' is the imaginary component of the anomalous scattering and $Z_{\rm eff}$ is the effective atomic scattering factor (6.7 for proteins). A frequency-weighted average of 7.8 non-H atoms per residue was used in the calculation of N_T.

Table 2
Phasing and automated model-building statistics.

	S-SAD	Se-SAD	SIRAS
f'	0.334	−0.790	−0.790
f''	0.557	1.137	1.137
Anomalous signal estimate† (%)	0.86	1.60	1.60
Isomorphous signal estimate‡ (%)	—	—	12.7
FOM before *RESOLVE*	0.31	0.29	0.35
FOM after *RESOLVE*	0.53	0.51	0.60
Residues built§	354 (79.4%)	337 (75.6%)	385 (86.3%)
Full side chains	305 (68.4%)	313 (70.2%)	345 (77.3%)
Truncated to alanine	44 (9.9%)	20 (4.5%)	37 (8.3%)
Truncated to glycine	5 (1.1%)	4 (0.9%)	3 (0.7%)
R.m.s.d. (Å)			
C^{α}	0.48¶	0.55††	0.52¶
Backbone	0.53¶	0.65††	0.55¶

† Calculated by $\langle \Delta F^{\pm}/F_T \rangle = (N_A/2N_T) - (2f''/Z_{\rm eff})$, where N_A and N_T are the number of anomalous scatters and the number of non-H atoms in the asymmetric unit, respectively, f'' is the imaginary component of the anomalous scattering and $Z_{\rm eff}$ is the effective atomic scattering factor (6.7 for proteins). ‡ Calculated by $\langle \Delta F_H/F_T \rangle = (N_H/2N_T) - [(f^{o}_{\rm Se} - f^{o}_{\rm S})/Z_{\rm eff}]$, where N_H and N_T are the number of heavy atoms and the number of non-H atoms in the asymmetric unit, respectively, $f^{o}_{\rm Se}$ and $f^{o}_{\rm S}$ are the scattering factors for selenium and sulfur, respectively, and $Z_{\rm eff}$ is the effective atomic scattering factor (6.7 for proteins). § Percentages were calculated omitting the nine amino-acid affinity tag, which was not observed in any of the previously reported EAS structures. ¶ Compared with the refined S-Met structure. †† Compared with the refined Se-Met structure.

phase-probability distributions by exploiting the anomalous differences in the Cu $K\alpha$ Se-Met EAS data. Although only 16 methionine residues are present in EAS, the positions of 19 anomalous scatters were sought, as there are also three cysteine residues with an appreciable anomalous signal at Cu $K\alpha$ wavelength. Using the basic *SOLVE*/*RESOLVE* strategy described above, 17 anomalous scattering sites were found, which were later determined to be 15 selenium sites and two sulfur sites. For the purposes of phase calculations, all 17 sites were considered to be selenium. The resulting electron-density map was of sufficient quality for the *RESOLVE* automated model-building algorithm to correctly build 337 residues of the protein (Table 2; Fig. 2).

2.4.4. Selenium SIRAS. The *SOLVE* algorithm was used to search for 16 Se-atom positions and calculate phase-probability distributions by exploiting the isomorphous differences between the S-Met and Se-Met data sets as well as the anomalous differences in the Se-Met data set. Using the basic *SOLVE*/*RESOLVE* strategy described above, 16 peaks were found by *SOLVE*, 15 of which were later confirmed as correct Se-atom sites. Using all 16 sites, the *SOLVE*/*RESOLVE* combination was able to correctly build 345 residues of the protein (Table 2; Fig. 2).

2.5. Structure refinement of the native and derivative EAS data and assessment of *RESOLVE* models

The known structure of EAS (Lemke & Howell, 2002) was used to derive models for the S-SAD and Se-SAD Cu $K\alpha$ data. Inspection of the initial maps revealed that shifts of approximately 1 Å were needed to align the known EAS model to the S-SAD and Se-SAD density. This shift is thought to be the consequence on non-isomorphism in the *c*-axis dimension. The known EAS structure was therefore superimposed onto the *RESOLVE* fragments and subsequently refined using the simulated-annealing, individual *B*-factor refinement and energy-minimization protocols incorporated in the program *CNS* (Brünger *et al.*, 1998). A maximum-likelihood target (Adams *et al.*, 1999; Pannu *et al.*, 1998) and a flat bulk-solvent correction were used. No σ or resolution cutoffs were applied to the data. 10% of each data set was omitted from the refinement for the calculation of $R_{\rm free}$. Each round of refinement was alternated with a round of manual rebuilding using *TURBO-FRODO* (Roussel & Cambillau, 1991). The structures were refined to the point that they could be used to assess the quality of the models generated by *RESOLVE*. The final S-Met and Se-Met structures were refined to an R and $R_{\rm free}$ of 18.5 and 21.4%, and 20.1% and 23.9%, respectively. Root-mean-square deviations (r.m.s.d.s) of corresponding fragments between the *RESOLVE* and refined models were calculated using *SWISS-PDB VIEWER* (Guex & Peitsch, 1997) (Table 2).

3. Discussion

The results of this work clearly demonstrate that with minimal user intervention, S-SAD, Se-SAD and S/Se-SIRAS data collected using Cu $K\alpha$ radiation can be used for *ab initio* structure determination through largely automated methods. Although there are other program packages that could have been used in this work, *SnB* and *SOLVE*/*RESOLVE* were used for their combination of power and automation. The three major steps used to generate model structures were substructure determination, map generation and model building. The results of each of these steps are discussed below.

The S-SAD, Se-SAD and S/Se-SIR *SnB* substructure-determination success rates were 0.17, 2.48 and 0.44%, respectively. Given that the theoretical isomorphous signal obtainable *via* S/Se-SIR is much higher than the theoretical anomalous signal obtainable *via* Se-SAD, the relatively low S/Se-SIR success rate was somewhat surprising. We believe that this lower success rate is largely a consequence of non-isomorphism between the two crystals and of differing systematic and random errors during the respective data collections. As demonstrated previously, the redundancy and resolution of the data will also adversely affect the *SnB* success rate (Howell *et al.*, 2000).

The direct-methods approach of *SnB* and the Patterson method approach of *SOLVE* were equally capable of determining the Se-atom substructure *via* Se-SAD and Se-SIR/Se-SIRAS. In order to present the simplest and most automated mode of structure determination, the *SOLVE* selenium-substructure determinations are reported. In our hands *SOLVE* was not able to determine the S-atom substructure, while *SnB* was capable of exploiting the very small anomalous signal to identify the sulfur positions.

The electron-density maps generated by *SOLVE* and *RESOLVE* were of very high quality (Fig. 3), particularly given the relatively weak signals from which they were

Table 3
Methionine and cysteine content of selected proteomes.

Values acquired from the EMBL–EBI web page at http://www.ebi.ac.uk/proteome.

Species	Methionine (%)	Cysteine (%)	Combined (%)
Eukaryotes			
Arabidopsis thaliana	2.45	1.84	4.29
Caenorhabditis elegans	2.61	2.05	4.66
Drosophils melanogaster	2.36	1.87	4.23
Homo sapiens	2.14	2.23	4.37
Saccharomyces cerevisiae	2.08	1.30	3.38
Archea			
Archaeoglobus fulgidus	2.62	1.18	3.80
Methanobacterium thermoautotrophicum	3.06	1.21	3.27
Pyrococcus abyssi	2.40	0.55	2.95
Sulfolobus solfataricus	2.20	0.62	2.82
Thermoplasmum acidophilum	3.20	0.60	3.80
Bacteria			
Bacillus subtillis	2.77	0.80	3.57
E. coli K-12	2.80	1.16	3.96
Haemophilus influenzae	2.42	1.03	3.45
Streptococcus pneumoniae TIGR4	2.47	0.60	3.07
Vibrio cholerae	2.73	1.05	3.78

calculated. Not surprisingly, the SIRAS phases were the best quality of the three, as measured by the figure of merit (FOM). This is likely to be the result of the combination of the S/Se isomorphous and Se anomalous signals. Somewhat unexpectedly, however, even though the expected selenium anomalous signal is double that of the sulfur (Fig. 4; Table 2), the S-SAD phases were marginally *better* than the Se-SAD phases. We attribute this disparity to the lower quality of the Se-Met data relative to the S-Met data, as evidenced by the higher $R_{\rm merge}$ and lower $I/\sigma(I)$ statistics (Table 1).

The percentage of the structure modeled by the automated building algorithm of *RESOLVE* correlates well with the quality of the electron-density maps (as described above). The SIRAS, S-SAD and Se-SAD *RESOLVE* models are 86.3, 79.4 and 75.6% complete, respectively (Fig. 2). Although a small number of the residues were truncated to either alanine or glycine, no residues were incorrectly assigned. The comparison of the *RESOLVE* models to the refined S-Met and/or Se-Met structures yields r.m.s.d.s of approximately 0.5 Å, indicating a very good agreement between the automatically built models and the refined structures. Any of the *RESOLVE* models could have been built and refined to yield complete EAS structures.

We therefore suggest that the *ab initio* structure determination of native or selenomethionine-derivatized structures using Cu $K\alpha$ radiation may be of general use where well diffracting protein crystals of sufficient methionine and/or selenomethionine content are available. The protein used for this work contains 16 methionines residues and three cysteines in 455 residues, or 3.52 and 0.66%, respectively. The fact that these values are comparable to many species' averages (Table 3) suggests that many proteins could be solved using the anomalous signal from Cu $K\alpha$ radiation as described in the experiments reported here.

4. Conclusions

S-SAD, Se-SAD and S/Se-SIRAS data collected with Cu $K\alpha$ radiation can be used to produce interpretable electron-density maps from well diffracting crystals of average methionine or cysteine content. While the Se-SAD and S/Se-SIRAS applications described here could save a trip to the synchrotron for crystallographers who have produced selenomethionine-derivatized protein crystals, the S-SAD application may avoid the requirement for synchrotron radiation as well as the need to incorporate selenium or other heavy atoms into the protein altogether. We anticipate that this method will gain in popularity, since all that is really required is an accurate diffraction experiment.

This work was supported in part by grants from the National Institutes of Health, GM-46733 (GDS) and the Canadian Institutes of Health Research, MT13337 (PLH) and studentship awards from the Canadian Institutes of Health Research, the University of Toronto and the Hospital for Sick Children (CTL).

References

Adams, P. D., Pannu, N. S., Read, R. J. & Brunger, A. T. (1999). *Acta Cryst.* D**55**, 181–190.
Blessing, R. H. (1989). *J. Appl. Cryst.* **22**, 396–397.
Blessing, R. H. & Smith, G. D. (1999). *J. Appl. Cryst.* **32**, 664–670.
Brünger, A. T., Adams, P. D., Clore, G. M., DeLano, W. L., Gros, P., Grosse-Kunstleve, R. W., Jiang, J. S., Kuszewski, J., Nilges, M., Pannu, N. S., Read, R. J., Rice, L. M., Simonson, T. & Warren, G. L. (1998). *Acta Cryst.* D**54**, 905–921.
Dauter, Z., Dauter, M., de La Fortelle, E., Bricogne, G. & Sheldrick, G. M. (1999). *J. Mol. Biol.* **289**, 83–92.
Deacon, A. M. & Ealick, S. E. (1999). *Structure*, **7**, R161–R166.
Gordon, E. J., Leonard, G. A., McSweeney, S. & Zagalsky, P. F. (2001). *Acta Cryst.* D**57**, 1230–1237.
Guex, N. & Peitsch, M. C. (1997). *Electrophoresis*, **18**, 2714–2723.
Hendrickson, W. A. & Teeter, M. M. (1981). *Nature (London)*, **290**, 103–113.
Howell, P. L., Blessing, R. H., Smith, G. D. & Weeks, C. M. (2000). *Acta Cryst.* D**56**, 604–617.
Lemke, C. T. & Howell, P. L. (2001). *Structure*, **9**, 1153–1164.
Lemke, C. T. & Howell, P. L. (2002). *J. Biol. Chem.* **277**, 13074–13081.
Lemke, C., Yeung, M. & Howell, P. L. (1999). *Acta Cryst.* D**55**, 2028–2030.
Liu, Z. J., Vysotski, E. S., Chen, C. J., Rose, J. P., Lee, J. & Wang, B. C. (2000). *Protein Sci.* **9**, 2085–2093.
Micossi, E., Hunter, W. N. & Leonard, G. A. (2002). *Acta Cryst.* D**58**, 21–28.
Pannu, N. S., Murshudov, G. N., Dodson, E. J. & Read, R. J. (1998). *Acta Cryst.* D**54**, 1285–1294.
Pflugrath, J. W. (1999). *Acta Cryst.* D**55**, 1718–1725.
Ramakrishnan, V. & Biou, V. (1997). *Methods Enzymol.* **276**, 538–557.
Roussel, A. & Cambillau, C. (1991). *Silicon Graphics Geometry Partners Directory*, p. 81. Mountain View, CA, USA: Silicon Graphics Corporation.
Sheldrick, G. M. & Schneider, T. R. (1997). *Methods Enzymol.* **227**, 319–343.
Smith, G. D. (2002). *J. Appl. Cryst.* **35**, 368–370.
Terwilliger, T. C. & Berendzen, J. (1999). *Acta Cryst.* D**55**, 849–861.
Weeks, C. M. & Miller, R. (1999). *J. Appl. Cryst.* **32**, 120–124.
Yang, C. & Pflugrath, J. W. (2001). *Acta Cryst.* D**57**, 1480–1490.